International Journal of Applied Mechanics
Vol. 8, No. 7 (2016) 1640006 (13 pages)

DOI: 10.1142/S1758825116400068

World Scientific
www.worldscientific.com

Energy Absorption of Thermoplastic Polyurethane Lattice Structures via 3D Printing: Modeling and Prediction

Fei Shen*, Shangqin Yuan*, Yanchunni Guo*, Bo Zhao*,
Jiaming Bai†, Mahan Qwamizadeh*, Chee Kai Chua*,
Jun Wei* and Kun Zhou*,‡

*School of Mechanical and Aerospace Engineering
Nanyang Technological University
Singapore 639798, Singapore

†Singapore Institute of Manufacturing Technology
71 Nanyang Drive, Singapore 638075, Singapore
‡kzhou@ntu.edu.sg

Received 19 September 2016
Revised 1 November 2016
Accepted 2 November 2016
Published 16 December 2016

This work investigates the energy absorption capacity of polymeric lattice structures through a systemic manufacturing, testing and modeling approaches. The lattice structures are designed to possess periodic cubic geometry with optimized spherical shells located at the cubic corners, and thermoplastic polyurethane (TPU) powders are used to fabricate such structures via selective laser sintering, a type of powder-based 3D printing technology. A hyperelastic model that considers the mullins effect and describes the cyclic compression stress–strain behavior of TPU is developed to simulate the mechanical response of its 3D-printed lattice structures under cyclic compression loading. After the validation of the model for printed structure, it is used to predict the energy absorption capacity of various designed structures.

Keywords: Lattice structures; energy absorption; 3D printing; thermoplastic polyurethane; finite element method.

1. Introduction

Lattice structures composed by periodic or stochastic arrangements of unit cells can offer unique functional characteristics allowing design freedom beyond the capability of bulk materials [Zheng *et al.*, 2014; Chen *et al.*, 2015]. By selection of cell topologies, geometrical parameters and materials, such structures can address a range of structural requirements from high compliance to high specific strength. Therefore, these structures attract great interests from researchers. In the recent

‡Corresponding author.

years, additive manufacturing (AM) [Chua *et al.*, 2010; Roberson *et al.*, 2013; Cruz Sanchez *et al.*, 2014; Yap and Yeong, 2014; Khoo *et al.*, 2015; Yap and Yeong, 2015; Bos *et al.*, 2016; Francis and Jain, 2016] provides an exceptional opportunity for the manufacture of these structures with complex configurations.

The mechanical behavior of lattice structures constituted by truss-based unit cells has been extensively investigated in the last decade. Plenty of materials such as metals, polymers and ceramics are used to fabricate such structures. Depending on its geometric topology, the unit cell can exhibit stretch-dominated or bend-dominated behavior under compression loading. The first stage of stress–strain behavior under compression exhibits a linear elastic response and is followed by a stress plateau or a slight drop induced by the buckling of trusses. After the neighboring trusses meet and touch, the densification causes the stress to increase steeply. With the knowledge of the stress and strain, the energy absorption capacity and the failure modes can be studied. The absorbed energy per unit volume in the loading process is the area under the stress–strain curve. The investigation results of energy absorption can be used to guide the structural design and the optimization for a high capacity of energy absorption [Avalle *et al.*, 2001; Hammetter *et al.*, 2013; Mazur *et al.*, 2016; Ozdemir *et al.*, 2016].

A new group of soft lattice structures was designed to possess periodic geometry of spherical shells which could be arranged in the patterns of simple cubic, body-centered cubic or face-centered cubic [Babaee *et al.*, 2013]. Soft rubber is used in the manufacture so that these structures have excellent behavior of recovery after the unloading. The structure with body-centered cubic pattern exhibited a unique behavior of negative Poisson's ratio under compression, which was also called auxetic behavior. It was attributed to the local buckling of spherical shells. The instability-induced pattern transformation of periodic structures was also used in the application of controlling the propagation of sound wave [Casadei and Bertoldi, 2014; Shim *et al.*, 2015; Babaee *et al.*, 2016].

However, the aforementioned investigations on the energy absorption have mainly conducted for the truss-based structures, but rarely reported for the spherical-shell ones. In fact, the energy absorption behavior of spherical-shell structures made of soft materials is repeated due to the excellent recoverable performance under cyclic compression. In order to reduce the above gap, it is necessary to provide a proper model to predict the mechanical behavior of these structures. It can be used to optimize different types of designs for high-performance energy absorption.

The present paper focuses on the energy absorption capacity of polymeric lattice structures possessing periodic cubic geometry with spherical shells located at the cubic corners. Thermoplastic polyurethane (TPU) [Feng and Ye, 2011; Plummer *et al.*, 2012; Vasquez *et al.*, 2014; Yuan *et al.*, 2016b] with excellent elongation at break and high recoverable performance under cyclic loading is used to fabricate such structures through selective laser sintering (SLS) [Tan *et al.*, 2005; Maekawa *et al.*, 2012; Bai *et al.*, 2014, 2015; Joshi and Sheikh, 2015; Hung *et al.*, 2016; Tan

et al., 2016a; Tan *et al.*, 2016b], a type of powder-based three-dimensional (3D) printing technology. A hyperelastic model considering the mullins effect is develop to describe the cyclic compression behavior of TPU. This model is used to simulate the cyclic compression behavior of lattice structures. After the validation of this model through cyclic compression testing of 3D-printed structure, the energy absorption capacity is studied by this numerical method. The effects of compressive strains and geometric parameters of spherical shells are also investigated.

2. Designs and 3D Printing

The schematic view of lattice structures is illustrated in Fig. 1(a). The fundamental unit is a spherical shell with holes, half of which is shown in Fig. 1(b). The simple cubic pattern, one spherical shell located at each corner of the cubic, is employed in this study.

For a spherical shell, the outer radius R_0 and inner radius R_1 are two important geometric parameters, as indicated in Fig. 1(b). The porosity of a spherical shell is controlled by both radii, defined as

$$\phi = 1 - \frac{V_u}{V_s}, \tag{1}$$

where V_u and V_s are the volumes of the spherical shell and intact sphere respectively. For the whole lattice structure, the numbers of layers of spherical shells in the x-, y- and z-directions are set as 5, 6 and 3 in this study. The distance l between the centers of two adjacent shells is the last parameter to determine the geometry. The global porosity of the lattice structure is defined as

$$\phi_g = 1 - \frac{V_l}{V}, \tag{2}$$

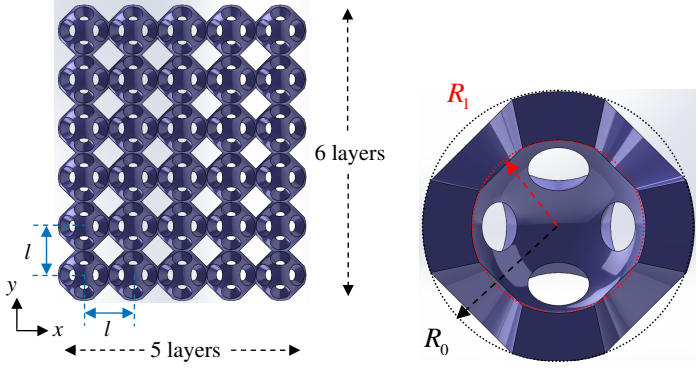

(a) (b)

Fig. 1. Schematic views of (a) spherical-shell lattice structure and (b) half of the spherical shell.

Table 1. Geometric parameters of various lattice structures.

Design	l (mm)	R_0 (mm)	R_1 (mm)	ϕ	ϕ_g
A	11.578	6.052	5.696	0.918	0.957
B	11.578	6.052	5.052	0.781	0.880
C	11.578	6.052	4.612	0.715	0.838
D	11.578	6.052	4.230	0.658	0.805
E	11.578	6.052	3.883	0.600	0.783
F	11.578	6.052	3.415	0.540	0.737
G	11.578	6.052	3.028	0.500	0.713
H	11.578	6.052	2.552	0.457	0.688

where V_l is the total volume of the lattice structure and V is the volume of the cuboids containing the whole structure. This porosity is different from that of spherical shells due to the simple cubic pattern.

In order to consider the effect of porosity, various designs of spherical shells with different inner radius R_1 are studied, the parameters of which are listed in Table 1. The other two parameters R_0 and l are fixed for simplicity. Two porosities for these designs are calculated, as listed in Table 1.

The material TPU is used to fabricate such structures. Generally, this material represents a class of randomly segmented copolymers consisting of hard and soft segments at the room temperature. The hard segments are acting as the physical crosslinks, which are immersed in the soft segment matrix. The combination of two types of segments imparts the material mechanical performance, resulting in the extensive applications in the industries. In this study, TPU powders (DESMOSINT X92) used for laser sintering are purchased from BASF Germany. Its density is about $0.65\,\mathrm{g/cm^3}$ and the melting temperature is around 150°C. Design E in Table 1 is produced by SLS on EOS P395 system (EOS GmbH Munch, Germany). The process parameters listed in Table 2 are optimized considering the size range, the input energy of melting and recrystallization behavior in the manufacture. The double contour and edge controls are applied in order to improve the dimensional accuracy and retain the edge features. After the laser sintering, the post-processes via sand-blasting and ultra-sonication are used to remove the residual powders on the internal surfaces. More details are presented in the works of Yuan *et al.* [2016a, 2016b].

Table 2. Laser sintering parameters.

Process parameter	Value
Laser power	
Hatching (W)	12
Contour 1, Contour 2 (W)	12, 12
Edge 1, Edge 2 (W)	14, 14
Other parameters	
Scanning speed (mm/s)	3000
Hatching spacing (mm)	0.1
Bed temperature (°C)	96
Chamber temperature (°C)	60
Layer thickness (μm)	100

3. Numerical Simulation

3.1. *Constitutive models*

The uniaxial compression testing of the material TPU are conducted under room temperature to obtain the stress–strain behavior. Cylindrical sample with the diameter of 15 mm is subjected to loading-unloading cycles in its axial direction. A small loading rate, $5 \times 10^{-4}\,\mathrm{s}^{-1}$, is used in four cycles to make sure that the time dependence is not significant. The maximum nominal strain for each cycle is $\varepsilon_{\max} = 0.25$, as shown in Fig. 2. It is worth noting that the hysteresis phenomenon in each cycle is obvious, illustrating that the energy absorption due to the frictional sliding between the long molecules. The last three curves are close to each other and the curve of the fourth cycle is used to calibrate the material parameters in the constitutive model.

In this study, the constitutive model proposed by Qi and Boyce [2005] is not used due to its complexity. Alternatively, the common hyperelastic model combined with the mullins effect is adopted to simulate the hysteresis behavior of the stable stress–strain curve. The polynomial strain energy potential with order one is used as follows:

$$U = C_{10}(\bar{I}_1 - 3) + C_{01}(\bar{I}_2 - 3), \tag{3}$$

where C_{10} and C_{01} are material parameters determined by the uniaxial compression testing; $\bar{I}_1$ and $\bar{I}_2$ are the first and second deviatoric strain invariants, respectively. The volume incompressibility is assumed. For this material, the transition temperature is about $-40°$C and the melting temperature is about 150°C, which indicates

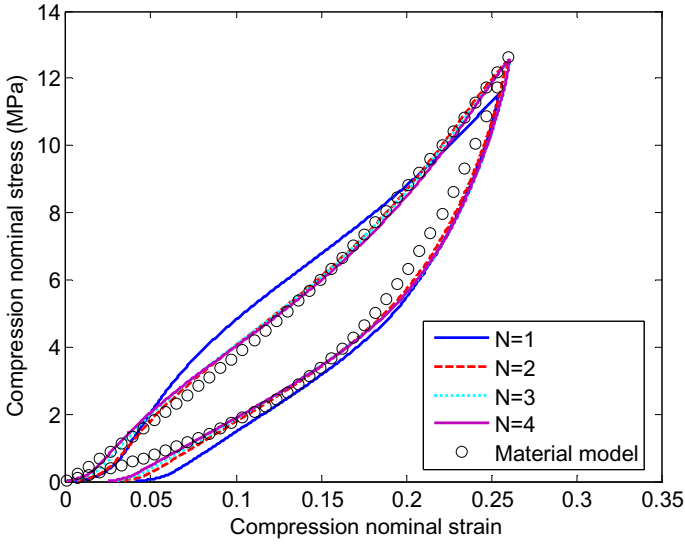

Fig. 2. TPU material cyclic compression stress–strain curves.

that the material is in rubbery state under the room temperature emphasizing that the assumptions are reasonable. The model for the mullins effect was developed by Ogden and Roxburgh [1999] to describe the stress softening of materials under cyclic loading. A damage variable, ranging from 1 to 1, is defined to modify the strain energy potential in the hyperelastic model and varies continuously during the loading process.

The common hyperelastic model and the mullins effect model have been implemented in the finite element packages Abaqus (Version 6.13, 2016). There is no need of coding to implement both models. Figure 2 illustrates the comparison between the experimental and numerical results. In the testing, the material cannot recover completely after the unloading. Small residual strain is observed, which is called permanent set. Although the model cannot capture this behavior, it gives a good prediction of material stress–strain behavior under cyclic loading.

3.2. *Finite element model*

The nonlinear commercial finite element package Abaqus is employed to simulate the compression behavior of lattice structures. Due to the symmetry, only one eighth of the whole structure is modeled. The symmetrical boundary constraints in the x-, y- and z-directions are applied on the corresponding surfaces. A rigid plane is built on the top of the structure as the compression plate. The contact between the rigid plane and the structure is defined using the master–slave algorithm for contact between surfaces. The rigid plane is defined as the master surface and part of the surfaces of lattice structures are defined as the slave surface. The default hard contact is used for the normal behavior and the friction between the contact surfaces is ignored. Besides, a general contact interaction is defined to model the possible self-contact between the different spherical shells under the compression. Four-node linear tetrahedron element with hybrid formulation is employed for the volume incompressibility assumption. The mesh convergence of the simulation is conducted by trial and error method to obtain the stable numerical results. The final mesh size is about 0.4 mm and the total number of elements of each design is around 200,000.

In the simulation, the vertical displacement was applied on the reference point of the upper rigid plane. Due to the vertical symmetry, this displacement is half of the experimental value. The reaction force of this reference point is a critical result, which represents the force on the lattice structures. The total force is four times the reaction force obtained from the simulation. Another result is the total energy absorbed during the cyclic loading, which can be calculated from the simulation result multiplied by eight.

It is worth noting that the buckling phenomenon of the lattice structure is not observed in the testing. Two main reasons may be attributed: (a) the simple cubic pattern inhibits the rotation of each spherical shell; (b) the finite boundary will

depress the occurrence of buckling. No plateau is found in the load-displacement curves obtained from the testing, which validates the nonexistence of buckling. Therefore, the buckling and post-buckling analyses are not included in the simulation.

4. Results

4.1. *Modeling verification*

The compression testing of the 3D-printed lattice structure (Design E) is used to validate the modeling. The cyclic loading with a small loading rate of $1.5 \times 10^{-3}\,\mathrm{s}^{-1}$ is applied in the y-direction of the structure, as shown in Fig. 3(a). The maximum compression displacement is set as about 17 mm to ensure that the maximum nominal strain is 25%. The deformation of the structure under the maximum loading is illustrated in Fig. 3(b). Nearly all the spherical shells have identical shapes after deformation. The dimension shrinkage is not observed along the x-direction, which is different from that reported by Babaee *et al.* [2013]. The force–displacement data for four cycles are illustrated in Fig. 4. Under this strain rate, the difference is of insignificant between these curves. It should be noted that the area surrounded by the loading and unloading paths is the energy absorption in one cycle.

The predicted results of the load–displacement curve are compared with the experimental data, as depicted in Fig. 4. Some deviations occur in the last half portion of loading process and the first half portion of unloading process. The manufacturing errors of SLS may be a reason for this. The maximum forces of the fourth cycle and the calculated results are around 440 N and 490 N, respectively, leading to a deviation of about 10%. The model provides a reasonable prediction of the cyclic compression behavior of the lattice structure.

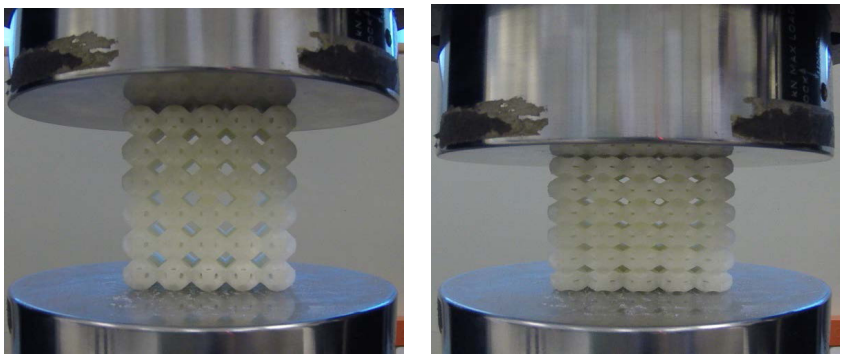

(a) $\varepsilon = 0$ (b) $\varepsilon = 0.25$

Fig. 3. Experiment at two times in one cycle for Design E.

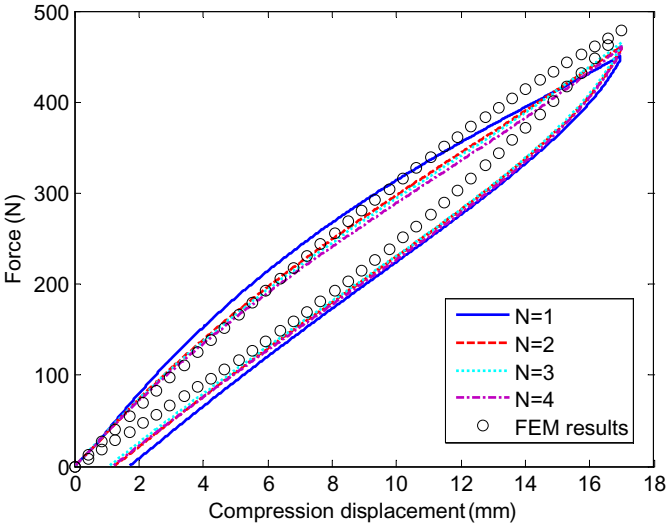

Fig. 4. Comparison of load–displacement curves for Design E.

4.2. *Energy absorption*

4.2.1. *Effect of strain*

The effect of strain on the energy absorption is analyzed numerically for these lattice structures. Due to different volumes or masses for the designs, the energy absorption per unit volume is used instead of the total absorbed energy, defined as

$$\psi = \frac{W_{\mathrm{d}}}{V} = \frac{\int_{1\,\mathrm{cycle}} F\mathrm{d}u}{V}, \tag{4}$$

where W_{d} is the total absorbed energy in one cycle. Variables F and u are the force and displacement, respectively. The energy absorption capacity at different strain is calculated and the results of Designs E and H are illustrated in Fig. 5. The maximum values of energy absorption per unit volume are 0.00494 and 0.01866, respectively. The relation between the energy absorption and the strain is nonlinear. When the compression strain is below 0.1, the increase of energy absorption is not significant. However, the energy absorption capacity increases quickly as the strain exceeds 0.1. Even though the magnitudes of energy absorption capacity are different for various designs, the trends as a function of strain are similar to each other.

4.2.2. *Effect of porosity*

The capacities of energy absorption are compared at the maximum strain 25%. The lattice structures are compressed to the same nominal strain. It should be noted that the materials are easier to move due to the more volume of voids for the structures with higher global porosity. The strength of whole structure decreases

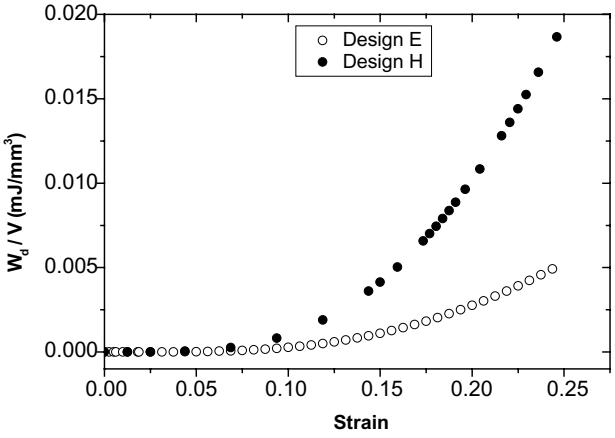

Fig. 5. Absorbed energy per unit volume as a function of strain for two designs.

with increasing porosity, which reduces the reaction force under the same maximum strain. As reported by Zheng *et al.* [2014], the traditional stretch-dominated lattice structures exhibit a linear relationship between the relative strength and relative density, $\sigma/\sigma_s \propto \rho/\rho_s$, where ρ and ρ_s are densities of the lattice structure and bulk material respectively and similar definitions for stresses σ and σ_s. In this study, the porosity has a linear but reverse relationship with relative density, in other words, $\phi_g = 1 - \rho/\rho_s$. The forces of eight designs are depicted as a function of porosity in Fig. 6. A polynomial function is used to fit this data:

$$F \propto (1 - \phi_g)^3. \tag{5}$$

The fitting shows that the strength of the spherical-shell lattice structures is more sensitive to its porosity than that of the traditional stretch-dominated ones.

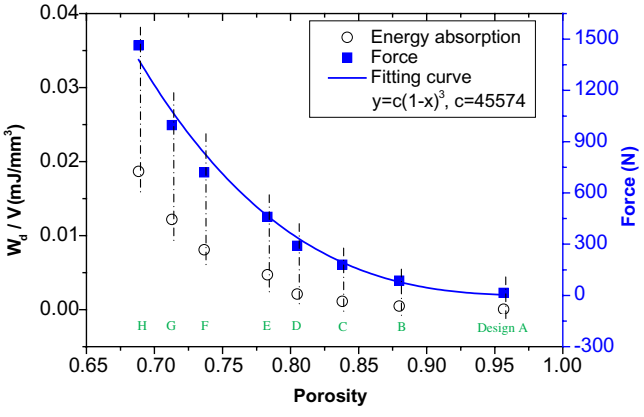

Fig. 6. Evolutions of energy absorption per unit volume and force as a function of porosity.

The energy absorption per unit volume decreases as the porosity increases, as shown in Fig. 6. The demand of light weight is conflictive with that of high capacity of energy absorption. Another trend is that the rate of decrease becomes small. The change of energy absorption with the increase of porosity is insignificant as the porosity is high. The maximum value of energy absorption per unit volume is about $0.02\,\mathrm{mJ/mm^3}$. It is necessary to emphasize that this result is obtained under quasi-static cyclic loadings and no failure happens, which is quite different from the impact testing [Stupak and Donovan, 1994; Ramakrishna *et al.*, 1995; Morye *et al.*, 2000; Wang *et al.*, 2015; Xiang *et al.*, 2015; Ding *et al.*, 2016]. If the lattice structures are compressed up to failure, the absorbed energy is defined as the area below the loading curve, which is greater than that surrounded by the loading and unloading curves. However, the structures cannot be used again after failure. In this study, the spherical-shell lattice structures are able to recover after the unloading, which indicates the repeated energy absorption of such structures.

5. Conclusion

The energy absorption capacity of spherical-shell lattice structures under cyclic compression loading is investigated through both experimental and numerical approaches. Such structures are constructed by periodically cubic arrangement of spherical shells and their radii are determined by the optimized design. TPU powders are used to manufacture the lattice structures via 3D printing. A hyperelastic model that considers the mullins effect is developed to describe the cyclic compression stress–strain behavior of TPU, which is used to simulate the cyclic compression behavior of lattice structures. The cyclic compression testing of the 3D-printed structure is conducted in order to validate the model. After that, the energy absorption capacity of various designed structures is predicted.

The present study provides a simple and effective method for the investigation of energy absorption capacity of 3D-printed lattice structures. The prediction shows a strong nonlinear relationship between the energy absorption capacity and the compression strain. Moreover, a cubic-like relationship between the compression force and the porosity is observed, which indicates that the strength of spherical-shell lattice structure is sensitive to the porosity. The energy absorption capacity decreases with the increase of porosity. The trend shows that the change of energy absorption with the increase of porosity is insignificant for the structures with high porosity.

Acknowledgments

The authors acknowledge the financial supports from the Agency for Science, Technology and Research, Singapore (SERC Grant No. 1325504106) and the Ministry of Education, Singapore (Academic Research Fund TIER 1 − RG174/15).

References

Avalle, M., Belingardi, G. and Montanini, R. [2001] "Characterization of polymeric structural foams under compressive impact loading by means of energy-absorption diagram," *International Journal of Impact Engineering* **25**(5), 455–472.

Babaee, S., Shim, J., Weaver, J. C., Chen, E. R., Patel, N. and Bertoldi, K. [2013] "3D Soft metamaterials with negative Poisson's ratio," *Adv. Mater.* **25**(36), 5044–5049.

Babaee, S., Viard, N., Wang, P., Fang, N. X. and Bertoldi, K. [2016] "Harnessing deformation to switch on and off the propagation of sound," *Adv. Mater.* **28**, 1631–1635.

Bai, J., Goodridge, R. D., Hague, R. J., Song, M. and Okamoto, M. [2014] "Influence of carbon nanotubes on the rheology and dynamic mechanical properties of polyamide-12 for laser sintering," *Polymer Testing* **36**, 95–100.

Bai, J., Goodridge, R. D., Yuan, S., Zhou, K., Chua, C. K. and Wei, J. [2015] "Thermal influence of CNT on the polyamide 12 nanocomposite for selective laser sintering," *Molecules* **20**(10), 19041–19050.

Bos, F., Wolfs, R., Ahmed, Z. and Salet, T. [2016] "Additive manufacturing of concrete in construction: Potentials and challenges of 3D concrete printing," *Virtual and Physical Prototyping*, 1–17.

Casadei, F. and Bertoldi, K. [2014] "Wave propagation in beams with periodic arrays of airfoil-shaped resonating units," *Journal of Sound and Vibration* **333**(24), 6532–6547.

Chen, M., Zhu, X., Lei, H., Chen, H. and Fang, D. [2015] "Effect of defect on the compressive response of sandwich structures with carbon fiber pyramidal truss cores," *International Journal of Applied Mechanics* **7**(01), 1550004.

Chua, C. K., Leong, K. F. and Lim, C. S. [2010] *Rapid Prototyping: Principles and Applications* (World Scientific).

Cruz Sanchez, F. A., Boudaoud, H., Muller, L. and Camargo, M. [2014] "Towards a standard experimental protocol for open source additive manufacturing," *Virtual and Physical Prototyping* **9**(3), 151–167.

Ding, Y., Wang, S., Zhao, K., Zheng, Z., Yang, L. and Yu, J. [2016] "Blast alleviation of cellular sacrificial cladding: A nonlinear plastic shock model," *International Journal of Applied Mechanics* **8**(4), 1650057.

Feng, F. and Ye, L. [2011] "Morphologies and mechanical properties of polylactide/thermoplastic polyurethane elastomer blends," *Journal of Applied Polymer Science* **119**(5), 2778–2783.

Francis, V. and Jain, P. K. [2016] "Experimental investigations on fused deposition modelling of polymer-layered silicate nanocomposite," *Virtual and Physical Prototyping* **11**(2), 109–121.

Hammetter, C. I., Rinaldi, R. G. and Zok, F. W. [2013] "Pyramidal lattice structures for high strength and energy absorption," *Journal of Applied Mechanics* **80**(4), 041015.

Hung, K. C., Tseng, C. S. and Hsu, S. H. [2016] "3D printing of polyurethane biomaterials," *Advances in Polyurethane Biomaterials*, 149–170.

Joshi, S. C. and Sheikh, A. A. [2015] "3D printing in aerospace and its long-term sustainability," *Virtual and Physical Prototyping* **10**(4), 175–185.

Khoo, Z. X., Teoh, J. E. M., Liu, Y., Chua, C. K., Yang, S., An, J. and Yeong, W. Y. [2015] "3D printing of smart materials: A review on recent progresses in 4D printing," *Virtual and Physical Prototyping* **10**(3), 103–122.

Maekawa, K., Yamasaki, K., Niizeki, T., Mita, M., Matsuba, Y., Terada, N. and Saito, H. [2012] "Drop-on-demand laser sintering with silver nanoparticles for electronics

packaging," *IEEE Transactions on Components, Packaging and Manufacturing Technology* **2**(5), 868–877.

Mazur, M., Leary, M., Sun, S., Vcelka, M., Shidid, D. and Brandt, M. [2016] "Deformation and failure behaviour of Ti-6Al-4V lattice structures manufactured by selective laser melting (SLM)," *The International Journal of Advanced Manufacturing Technology* **84**(5–8), 1391–1411.

Morye, S. S., Hine, P. J., Duckett, R. A., Carr, D. J. and Ward, I. M. [2000] "Modelling of the energy absorption by polymer composites upon ballistic impact," *Composites Science and Technology* **60**(14), 2631–2642.

Ogden, R. W. and Roxburgh, D. G. [1999] "A pseudo–elastic model for the Mullins effect in filled rubber," *Proceedings of the Royal Society of London A*: *Mathematical, Physical and Engineering Sciences* **455**, 2861–2877.

Ozdemir, Z., Hernandez-Nava, E., Tyas, A., Warren, J. A., Fay, S. D., Goodall, R. and Askes, H. [2016] "Energy absorption in lattice structures in dynamics: Experiments," *International Journal of Impact Engineering* **89**, 49–61.

Plummer, K., Vasquez, M., Majewski, C. and Hopkinson, N. [2012] "Study into the recyclability of a thermoplastic polyurethane powder for use in laser sintering," *Proceedings of the Institution of Mechanical Engineers*, *Part B*: *Journal of Engineering Manufacture* **226**(7), 1127–1135.

Qi, H. J. and Boyce, M. C. [2005] "Stress–strain behavior of thermoplastic polyurethanes," *Mechanics of Materials* **37**(8), 817–839.

Ramakrishna, S., Hamada, H., Maekawa, Z. and Sato, H. [1995] "Energy absorption behavior of carbon-fiber-reinforced thermoplastic composite tubes," *Journal of Thermoplastic Composite Materials* **8**(3), 323–344.

Roberson, D. A., Espalin, D. and Wicker, R. B. [2013] "3D printer selection: A decision-making evaluation and ranking model," *Virtual and Physical Prototyping* **8**(3), 201–212.

Shim, J., Wang, P. and Bertoldi, K. [2015] "Harnessing instability-induced pattern transformation to design tunable phononic crystals," *International Journal of Solids and Structures* **58**, 52–61.

Stupak, P. R. and Donovan, J. A. [1994] "Deformation and energy absorption of polymer foams as a function of 2D indenter and absorber geometries," *Polymer Engineering & Science* **34**(10), 857–864.

Tan, K. H., Chua, C. K., Leong, K. F., Cheah, C. M., Gui, W. S., Tan, W. S. and Wiria, F. E. [2005] "Selective laser sintering of biocompatible polymers for applications in tissue engineering," *Bio-Medical Materials and Engineering* **15**(1), 113–124.

Tan, H. W., Tran, T. and Chua, C. K. [2016a] "A review of printed passive electronic components through fully additive manufacturing methods," *Virtual and Physical Prototyping* **11**(4), 1–18.

Tan, W. S., Chua, C. K., Chong, T. H., Fane, A. G. and Jia, A. [2016b] "3D printing by selective laser sintering of polypropylene feed channel spacers for spiral wound membrane modules for the water industry," *Virtual and Physical Prototyping* **11**(3), 151–158.

Vasquez, G. M., Majewski, C. E., Haworth, B. and Hopkinson, N. [2014] "A targeted material selection process for polymers in laser sintering," *Additive Manufacturing* **1**, 127–138.

Wang, P., Zhang, X., Zhang, H., Li, X., He, P., Lu, G. and Yang, J. [2015] "Energy absorption mechanisms of modified double-aluminum layers under low-velocity impact," *International Journal of Applied Mechanics* **7**(06), 1550086.

Xiang, Y., Wang, M., Yu, T. and Yang, L. [2015] "Key performance indicators of tubes and foam-filled tubes used as energy absorbers," *International Journal of Applied Mechanics* **7**(04), 1550060.

Yap, Y. L. and Yeong, W. Y. [2014] "Additive manufacture of fashion and jewellery products: A mini review," *Virtual and Physical Prototyping* **9**(3), 195–201.

Yap, Y. L. and Yeong, W. Y. [2015] "Shape recovery effect of 3D printed polymeric honeycomb," *Virtual and Physical Prototyping* **10**(2), 91–99.

Yuan, S., Bai, J., Chua, C. K., Wei, J. and Zhou, K. [2016a] "Highly enhanced thermal conductivity of thermoplastic nanocomposites with a low mass fraction of MWCNTs by a facilitated latex approach," *Composites Part A*: *Applied Science and Manufacturing* **90**, 699–710.

Yuan, S., Bai, J., Chua, C. K., Zhou, K. and Jun, W. [2016b] "Characterization of creeping and shape memory effect in laser sintered thermoplastic polyurethane," *Journal of Computing and Information Science in Engineering* **16**(4), 041007.

Zheng, X., Lee, H., Weisgraber, T. H., Shusteff, M., DeOtte, J., Duoss, E. B. and Kucheyev, S. O. [2014] "Ultralight, ultrastiff mechanical metamaterials," *Science* **344**(6190), 1373–1377.